Pergamon

Int. J. Heat Mass Transfer. Vol. 39, No. 3, pp. 511–525, 1996
Elsevier Science Ltd
Printed in Great Britain

0017–9310(95)00149–2

Unsteady mixed convection about a rotating circular cylinder with small fluctuations in the free-stream velocity

HOA D. NGUYEN, SEUNGHO PAIK and R. W. DOUGLASS
Idaho National Engineering Laboratory, P.O. Box 1625, Idaho Falls, ID 83415, U.S.A.

(*Received* 4 *May* 1994 *and in final form* 5 *April* 1995)

Abstract—Heat transfer from a rotating circular cylinder immersed in a spatially uniform, time-dependent convective environment is investigated numerically including the effects due to buoyancy force. The flow equations, based on the vorticity and stream function, are solved along with the energy equation by a hybrid spectral scheme that combines the Fourier spectral method in the angular direction and a spectral element method in the radial direction. Several cases are simulated for Grashof numbers up to 2×10^4, Reynolds numbers up to 200, and a range of speed of rotation from -0.5 to $+0.5$. The results show that vortex shedding is promoted by the cylinder rotation but is vanished by the presence of the buoyancy force. In opposing flows, the counter flow currents cause a large expansion of the streamlines and isotherms in the direction normal to the free stream velocity. These changes in the structure of the flow and the temperature fields greatly modify the heat flux along the surface of the cylinder and consequently, the heat transfer rate is strongly dependent upon Reynolds number, Grashof number, rotational speed, and the gravity direction. Effects due to flow pulsation are also reflected in the Nusselt number history in the form of periodic oscillations.

1. INTRODUCTION

Heat transfer and fluid flow associated with a circular cylinder has been, for several decades, a subject of great attention among applied mathematicians, fluid dynamicists and heat transfer analysts owing to its numerous engineering applications such as the cooling of electronic components, the cooling of hot wire anemometers and the lift enhancement as attributed to Magnus effects. It is of great theoretical interest as being a prototypical model for studying important aspects of unsteady flow separation where several fundamental questions remain open.

The literature on convection about a cylinder in an unbounded medium is rich [1]. However, it is not our objective to make this survey exhaustive but to briefly review some of the relevant work in this area. For a circular cylinder suspended in a uniform flow environment, both hydrodynamics and heat transfer have been well addressed by several researchers. Dennis and his co-workers [2] solved the steady problem for Reynolds numbers less than 40 using a semi-analytical method which combines Fourier analysis and finite differences in the angular and radial directions, respectively. Jain and Goel [3] and Karniadakis *et al.* [4] independently employed different formalisms and numerical approaches, vorticity-stream function vs primitive variables and finite differences vs spectral elements, to obtain results for Reynolds numbers up to 200 in an effort to investigate the heat transfer in the unsteady flow wake regime. Unlike the three aforementioned studies where the fluid motion is driven by an external force, Qureshi and Ahmad [5] considered the case in which convective currents are generated by buoyancy for Rayleigh numbers ranging from 10^{-2} to 10^7 by numerically integrating the equations via the SIMPLE algorithm. A conjugate problem of this kind was later treated by Kimura and Pop [6]. Both types of problems discussed thus far are nothing more than the extreme limits of a more general situation in which forced and free, that is, combined convection take place simultaneously. Jain and Lohar [7] and Badr [8] have, respectively, examined the problem in which the gravity was assumed to be parallel and perpendicular to the free stream velocity. The predicted flow patterns and the temperature fields reported in these two studies are remarkably different and the corresponding heat transfer rates show a strong dependence on the gravity direction. In a recent study, Ahmad and Qureshi [9] presented a unified formulation of the mixed convection problem which is applicable for arbitrary angle between the forced flow direction and gravity.

Despite a large number of solutions reported on a cylinder subjected to a uniform cross flow, very few were able to produce a non-symmetrical wake which occurs at Reynolds numbers above about 40, at the rear of the cylinder. Such a controversy has led many researchers to speculate that the phenomena is triggered by some sort of perturbation mechanism, the truncation error for example, rather than a hidden nature of the Navier–Stokes equations. Due to this difficulty, attempts have been made to excite the asymmetrical eddy in an attempt to study the flow

NOMENCLATURE

f_n, F_n sine and cosine components of the stream function, respectively
g gravity acceleration
g_n, G_n sine and cosine components of the vorticity, respectively
Gr Grashof number
h_n, H_n sine and cosine components of the temperature, respectively
N number of Fourier modes
N^e number of nodes in element e
Nu Nusselt number
Pr Prandtl number
r radial coordinate
R cylinder radius
Re Reynolds number
t time
$\mathbf{u}$ dimensionless velocity vector
U_∞ mean of the free stream velocity.

Greek symbols
α thermal diffusivity
β thermal expansion coefficient
γ speed of rotation
δ angle between free stream velocity and gravity
Δt time increment
θ angular coordinate
Θ temperature
ν kinematic viscosity
ρ fluid density
ϕ amplitude of oscillation, see equation (5b)
ψ stream function
ω vorticity
Ω_f Strouhal number.

Subscripts
w pertains to wall conditions
∞ pertains to free stream conditions
0 pertains to initial conditions.

Superscripts
k time level index.

behaviors in the wake. Patel [10] imposed a small disturbance by slowly rotating the cylinder for a short period of time and was able to generate a von Karman vortex street. Similar studies were also conducted by Badr *et al.* [11, 12], Ingham and Tang [13] and Tang and Ingham [14]. Forced convection heat transfer in this setting was analyzed by Badr and Dennis [15].

In spite of the fact that much understanding has been gained from the previous studies, our knowledge of convective phenomena about a cylinder is rather incomplete in the sense that answers to several questions are still lacking. Two of those questions including the effects of the buoyancy force on the heat transfer process under vortex shedding conditions and the response of the Nusselt number when the cylinder is exposed to turbulent flows where a large part of the unsteadiness arises from turbulent velocity fluctuations will be addressed in this study. In what follows we shall provide a detailed description of the problem followed by a mathematical model, based on the stream function-vorticity formulation, that governs the transport processes and an outline of the numerical methods for solving the equations, and finally results are presented to illustrate important features of the coupled fluid flow and heat transfer. Though a technical difficulty associated with the specification of the vorticity boundary conditions has long been acknowledged, an exact treatment will be used in this study to alleviate this difficulty in the hope of resolving the controversy about the existence of an asymmetrical wake behind a cylinder in uniform flows.

2. FORMULATION

2.1. *Problem statement*

The physical system to be considered is shown in Fig. 1 consisting of a circular cylinder of radius R exposed to an environment of infinite extent where the free stream velocity makes an angle δ with the gravitational acceleration vector. Initially, the fluid and the cylinder are at rest and both are at temperature Θ_0. Suddenly, the fluid acquires, in an impulsively started fashion, a uniform flow velocity which also has a small oscillation superimposed on it as described by $U_\infty[1+\phi\sin(2\pi\Omega_f t)]$ with Ω_f and ϕ being the Strouhal number and amplitude, respectively. Simultaneously, the cylinder instantaneously attains its rotational speed γ assuming that a positive value corresponds to counter-clockwise rotation and vice versa. In the same way, the temperature within the cylinder is raised to Θ_w, presumably higher than Θ_0, and remains so throughout the course of the simulation. As the cylinder and the fluid are in contact,

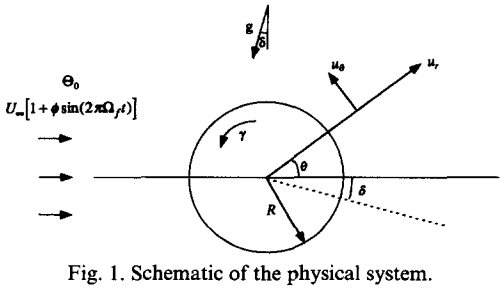

Fig. 1. Schematic of the physical system.

heat flow from the cylinder to the surrounding fluid creates a density variation which, in turn, gives rise to an additional mode of convective transport controlled by the buoyancy force. Whether or not the effects of free convection have profound influence is entirely dictated by the magnitude of the ratio of the Grashof number to the square of the Reynolds number and by the gravity direction. Depending on the orientation of the free stream velocity and the gravity, this directional dependence may lead to an enhancement or a degradation of heat transfer.

In principle, the time evolution of this mixed convection problem can be predicted by solving a system of equations derived from the well-known conservation law of mass, momentum, and energy. However, the inherent nonlinearities often make these equations intractable even with our latest advances in digital computers. In view of this, we shall simplify the problem using the following assumptions: (i) the Oberbeck–Boussinesq equations are valid implying that the fluid properties are constant except density in the body force term where it varies as a linear function of temperature, (ii) the length of the cylinder is much greater than its diameter so that end effects can safely be neglected and the transport processes become two-dimensional in r and θ and (iii) effects due to heat conduction in the cylinder interior are unimportant.

2.2. *Model equations*

Under the foregoing assumptions, the vorticity transport equation, the Poisson equation for the stream function, and the energy equation constitute a complete set of equations necessary for predicting the evolution of the convective phenomena described above. In dimensionless form, these equations are expressed as

$$\frac{\partial\omega}{\partial t}-\frac{1}{r}J(\psi,\omega)=\frac{2}{Re}\nabla^2\omega - \frac{Gr}{2Re^2}\left[\cos(\theta+\delta)\frac{\partial\Theta}{\partial r}-\frac{\sin(\theta+\delta)}{r}\frac{\partial\Theta}{\partial\theta}\right] \quad (1)$$

$$\nabla^2\psi=\omega \quad (2)$$

$$\frac{\partial\Theta}{\partial t}-\frac{1}{r}J(\psi,\Theta)=\frac{2}{RePr}\nabla^2\Theta \quad (3)$$

where ∇^2 is the Laplacian in cylindrical coordinates, and $J(\psi,\Theta)$ is the Jacobian. In these equations, the stream function ψ has been made dimensionless by RU_∞, the vorticity ω by U_∞/R, the time t by R/U_∞, the radial coordinate r by the cylinder radius R. The dimensionless groups Gr, Pr and Re, defined as $8g\beta(\Theta_w-\Theta_0)R^3/\nu^2$, ν/α and $2RU_\infty/\nu$, respectively, are known as the Grashof, Prandtl and Reynolds numbers. The stream function introduced above is related to the velocity by

$$\mathbf{u}=\frac{\mathbf{e}_r}{r}\frac{\partial\psi}{\partial\theta}-\mathbf{e}_\theta\frac{\partial\psi}{\partial r}. \quad (4)$$

The initial and boundary conditions to be imposed to equations (1)–(3) are the following:

$$\psi=0 \quad \frac{\partial\psi}{\partial r}=-\gamma \quad \Theta=1 \quad \text{at} \quad r=1 \quad (5a)$$

$$\psi=[1+\phi\sin(2\pi\Omega_t t)]r\sin\theta \quad \Theta=0 \quad \text{at} \quad r\to\infty, \quad (5b)$$

and

$$\omega=0 \quad \Theta=0 \quad \text{at} \quad t=0. \quad (5c)$$

In the next section, a hybrid spectral method is used in conjunction with a mixed time integration scheme to derive the discrete analogues of equations (1)–(3). One novel feature of the present solution technique is the use of the influence matrix technique to resolve the complications created by the lack of vorticity boundary conditions.

3. METHODS OF SOLUTION

3.1. *Temporal discretization*

Numerous explicit and implicit techniques exist for integrating the vorticity and the energy transport equations. Of particular interest in the present work is the semi-implicit scheme resulting from integration of the convective and diffusion terms by the Adams–Bashforth and the backward Euler methods, respectively. Upon applying these discretizations, there results a system of three linear, one-way coupled partial differential equations,

$$\left[\frac{Re}{2\Delta t}-\nabla^2\right]\omega^{k+1}=\frac{Re}{2\Delta t}\omega^k + \frac{Re}{4r}[3J(\psi^k,\omega^k)-J(\psi^{k-1},\omega^{k-1})] - \frac{Gr}{4Re}\left[\cos(\theta+\delta)\frac{\partial\Theta^{k+1}}{\partial r}-\frac{\sin(\theta+\delta)}{r}\frac{\partial\Theta^{k+1}}{\partial\theta}\right] \quad (6)$$

$$\nabla^2\psi^{k+1}=\omega^{k+1} \quad (7)$$

$$\left[\frac{RePr}{2\Delta t}-\nabla^2\right]\Theta^{k+1}=\frac{RePr}{2\Delta t}\Theta^k + \frac{RePr}{4r}[3J(\psi^k,\Theta^k)-J(\psi^{k-1},\Theta^{k-1})] \quad (8)$$

which are first-order accurate in time. Here, the superscript k represents the time level, and Δt denotes the time increment.

3.2. *Spatial discretization*

In the past, several researchers have obtained solutions for flow and heat transfer associated with a cylinder by means of a numerical scheme that utilizes the Fourier spectral method in the angular direction and a finite difference method in the radial direction. Unfortunately, the truncation errors in finite difference methods, as well as finite element methods, decay rather slowly and therefore the use of a partial spectral

algorithm would degrade the accuracy of the spectral methods. In order to preserve their accuracy, we shall ultilize a spectral method that combines Fourier spectral and spectral element methods.

3.2.1. *Fourier-spectral element method.* Following Badr [8], the stream function, vorticity, and the temperature are represented by Fourier expansions of the form:

$$\begin{Bmatrix} \psi(r,\theta) \\ \omega(r,\theta) \\ \Theta(r,\theta) \end{Bmatrix} = \frac{1}{2}\begin{Bmatrix} F_0(r) \\ G_0(r) \\ H_0(r) \end{Bmatrix} + \sum_{n=1}^{N} \begin{Bmatrix} F_n(r) \\ G_n(r) \\ H_n(r) \end{Bmatrix} \cos(n\theta) + \begin{Bmatrix} f_n(r) \\ g_n(r) \\ h_n(r) \end{Bmatrix} \sin(n\theta) \quad (9)$$

where $\{f_n\}$, $\{F_n\}$, $\{g_n\}$, $\{G_n\}$, $\{h_n\}$ and $\{H_n\}$ are six sets of unknown functions to be determined and N is the number of Fourier modes. Substituting these expressions into equations (6) and (8) and equating terms having a common factor in $\sin(n\theta)$ and $\cos(n\theta)$ yields equations for the expansion coefficients,

$$-\frac{d}{dr}\left(r\frac{dG_n^{k+1}}{dr}\right)+\left[\left(\frac{Re}{2\Delta t}\right)r+\frac{n^2}{r}\right]G_n^{k+1} = \left(\frac{Re}{2\Delta t}\right)rG_n^k - BG_n^{k+1} + \frac{Re}{8}[3SG_n^k - SG_n^{k-1}] \quad (10)$$

$$-\frac{d}{dr}\left(r\frac{dg_n^{k+1}}{dr}\right)+\left[\left(\frac{Re}{2\Delta t}\right)r+\frac{n^2}{r}\right]g_n^{k+1} = \left(\frac{Re}{2\Delta t}\right)rg_n^k - Bg_n^{k+1} + \frac{Re}{8}[3Sg_n^k - Sg_n^{k-1}] \quad (11)$$

$$-\frac{d}{dr}\left(r\frac{dH_n^{k+1}}{dr}\right)+\left[\left(\frac{RePr}{2\Delta t}\right)r+\frac{n^2}{r}\right]H_n^{k+1} = \left(\frac{RePr}{2\Delta t}\right)rH_n^k + \frac{RePr}{8}[3SH_n^k - SH_n^{k-1}] \quad (12)$$

$$-\frac{d}{dr}\left(r\frac{dh_n^{k+1}}{dr}\right)+\left[\left(\frac{RePr}{2\Delta t}\right)r+\frac{n^2}{r}\right]h_n^{k+1} = \left(\frac{RePr}{2\Delta t}\right)rh_n^k + \frac{RePr}{8}[3Sh_n^k - Sh_n^{k-1}] \quad (13)$$

where the convection terms are given in the Appendix.

Similar procedures can be applied to equation (7) to yield equations for the stream function components. The results are

$$-\frac{d}{dr}\left(r\frac{dF_n^{k+1}}{dr}\right)+\frac{n^2}{r}F_n^{k+1} = -rG_n^{k+1} \quad (14)$$

$$-\frac{d}{dr}\left(r\frac{df_n^{k+1}}{dr}\right)+\frac{n^2}{r}f_n^{k+1} = -rg_n^{k+1} \quad (15)$$

which can be solved once the vorticity components are known; thereby allowing the convection terms to be evaluated.

To complete the discretization process, a Galerkin-based spectral element method is applied to convert the above equations to their discrete equivalence. Because the method has been described at length in the literature (see Nguyen *et al.* [16]), details are omitted.

3.2.2. *Influence matrix technique.* As noted earlier, there is a technical difficulty associated with the overspecification and underspecification of the stream function and the vorticity boundary conditions, respectively. One way to circumvent this problem is to decompose each pair of $\{F_n^{k+1}, G_n^{k+1}\}$ and $\{f_n^{k+1}, g_n^{k+1}\}$ as a linear combination of solutions of auxiliary problems such that the overall solution satisfies both the differential equations as well as the boundary conditions. For the $\{F_n^{k+1}, G_n^{k+1}\}$ pair the solution is sought in the form

$$\begin{Bmatrix} F_n^{k+1} \\ G_n^{k+1} \end{Bmatrix} = \begin{Bmatrix} \Psi_0 \\ \Omega_0 \end{Bmatrix} + \chi \begin{Bmatrix} \Psi_1 \\ \Omega_1 \end{Bmatrix} \quad (16)$$

where Ψ_1 and Ω_1 are the solutions of the following problems:

$$\begin{cases} -\dfrac{d}{dr}\left(r\dfrac{d\Omega_1}{dr}\right)+\left[\left(\dfrac{Re}{2\Delta t}\right)r+\dfrac{n^2}{r}\right]\Omega_1 = 0 \\ -\dfrac{d}{dr}\left(r\dfrac{d\Psi_1}{dr}\right)+\dfrac{n^2}{r}\Psi_1 = -r\Omega_1 \\ \text{with} \\ \Omega_1(0) = 1 \quad \Omega_1(\infty) = 0 \\ \text{and} \quad \Psi_1(0) = 0 \quad \Psi_1(\infty) = 0. \end{cases} \quad (17)$$

and

$$\begin{cases} -\dfrac{d}{dr}\left(r\dfrac{d\Omega_0}{dr}\right)+\left[\left(\dfrac{Re}{2\Delta t}\right)r+\dfrac{n^2}{r}\right]\Omega_0 = \left(\dfrac{Re}{2\Delta t}\right)rG_n^k - BG_n^{k+1} + \dfrac{Re}{8}[3SG_n^k - SG_n^{k-1}] \\ -\dfrac{d}{dr}\left(r\dfrac{d\Psi_0}{dr}\right)+\dfrac{n^2}{r}\Psi_0 = -r\Omega_0, \\ \text{with} \\ \Omega_0(0) = 0 \quad \Omega_0(\infty) = 0 \\ \text{and} \quad \Psi_0(0) = 0 \quad \Psi_0(\infty) = 0. \end{cases} \quad (18)$$

The constant χ is determined from the no-slip condition that leads to

$$\chi = \frac{1}{d\Psi_1/dr|_{r=1}}(-2\gamma\delta_{0n} - d\Psi_0/dr|_{r=1}). \quad (19)$$

Likewise, the pair of solutions $\{f_n^{k+1}, g_n^{k+1}\}$ can be constructed in the manner described above except that $\gamma = 0$ for all n and $\Psi_0(\infty) = [1 + \phi \sin(2\pi\Omega_f t)]r_\infty$ for $n = 1$ and 0 otherwise.

4. RESULTS AND DISCUSSION

The contents of this section are organized into four parts: first, several tests for forced and mixed convection are performed to check the validity of the numerical algorithm developed earlier by comparing our predicted results against previously published solutions. Second, a special case for $Re = 200$ without cylinder rotation and free-stream fluctuation is simulated to see whether or not an asymmetric wake and/or vortex shedding occurs. Third, a parametric study is conducted to illustrate the behaviors of the flow and temperature fields with Gr, γ, Re and δ varying one at a time. Finally, we shall concentrate our efforts on interpreting the results, particularly the local and overall Nusselt numbers, so as to enhance our understanding of the thermal process under these conditions.

Listed in Tables 1 and 2 are the steady-state mean Nusselt numbers of forced and mixed convection, respectively. The values reported therein were determined based on the criteria that the change in the Nusselt number in 100 time steps is less than 10^{-3} or equivalently, the time variation of Nusselt number between two successive time steps is no greater than 10^{-5} on average. As one can see from Table 1, the overall agreement is very good, within a few percent. For $Re > 40$, our results are also in good agreement with the correlation

$$\overline{Nu} = 0.43 + 0.48\sqrt{Re}$$

that has been recommended by McAdams [17] for pure forced convection in air. With the effects of free convection, our data tend to fall between those predicted by Badr [8] and Gebhart *et al.* [18] at low Reynolds and Grashof numbers. As Re and Gr increase, however, our results tend to slightly overpredict the Nusselt number. Although the cause for this is unclear, it is likely attributed to how well the thin thermal layer is resolved. For numerical purposes, the computational domain in this study was truncated to 100 and was then divided into 25 elements with their sizes varies according to the exponential function with an exponential factor of 1.7. Within each element, five nodes were used and their locations were, in terms of their local coordinates ranging from -1 to 1, selected to correspond to the Gauss–Lobatto quadrature points, i.e. $\cos(i\pi/N^e)$. In this fashion, the nodal points are clustered in the vicinity of cylinder; hence, providing good spatial resolution to capture the transport behavior in the near-wall region.

Table 2. Mixed convection Nusselt numbers with $Pr = 0.7$, $\gamma = 0$ and $\delta = 0$

Re	Gr	Present	Gebhart *et al.* [18]	Badr [8]
1	4	1.09	1.19	0.96
5	100	1.89	1.99	1.82
20	1000	3.13	3.13	2.85
40	6400	4.59	4.46	4.17

Figures 2(a)–(c) depict the flow patterns and the temperature and the vorticity fields for the case of pure translation, referred to as case A in Table 3, with $Re = 200$. Because the early stage of the development is dominated by conduction, the presentation herein emphasizes the later periods during which the wake grows in an asymmetric fashion as a precursor for the eddies to break away from the cylinder surface. As noticed from the streamlines in Fig. 2(a) for $t = 10$, asymmetry has already appeared and is in the form of two eddies of unequal size. Data for later times, $t = 20$ and 30, reveal the growing of the eddies at a different pace which slowly erases the symmetry. Though the computations were extended to $t = 40$, no vortex shedding was seen and since the Nusselt number has already reached its steady-state value, the simulation was terminated. This decision was made on the basis that excessive computing time may be required before such a phenomena, believed to occur at much later time, can be observed. One important finding from these figures is a confirmation of the asymmetry which necessitates a full Fourier expansion as in equation (11) rather than just the sine components as some researchers had assumed in the past. Figures 3(a)–(c) show the development of the pressure, vorticity, and Nusselt number as a function of the angle (in radians) measured from the back stagnation point in the

Table 1. Forced convection Nusselt numbers with $\gamma = 0$†

Re	Pr 0.73	1	8
0.5	0.67 (0.66, 0.77)	0.72 (0.72, NA)	1.26 (1.22, NA)
2	1.03 (1.02, 1.11)	1.12 (1.12, NA)	2.07 (2.06, NA)
10	1.90 (1.90, 1.95)	2.10 (2.09, NA)	4.10 (4.16, NA)
20	2.53 (2.56, 2.58)	2.83 (2.83, NA)	5.68 (NA, NA)
40	3.47 (3.48, 3.47)	3.81 (NA, NA)	7.99 (NA, NA)
100	5.23 (NA, 5.23)		
200	7.10 (NA, 7.22)		

† First and second values in parentheses are from refs. [2] and [17], respectively.

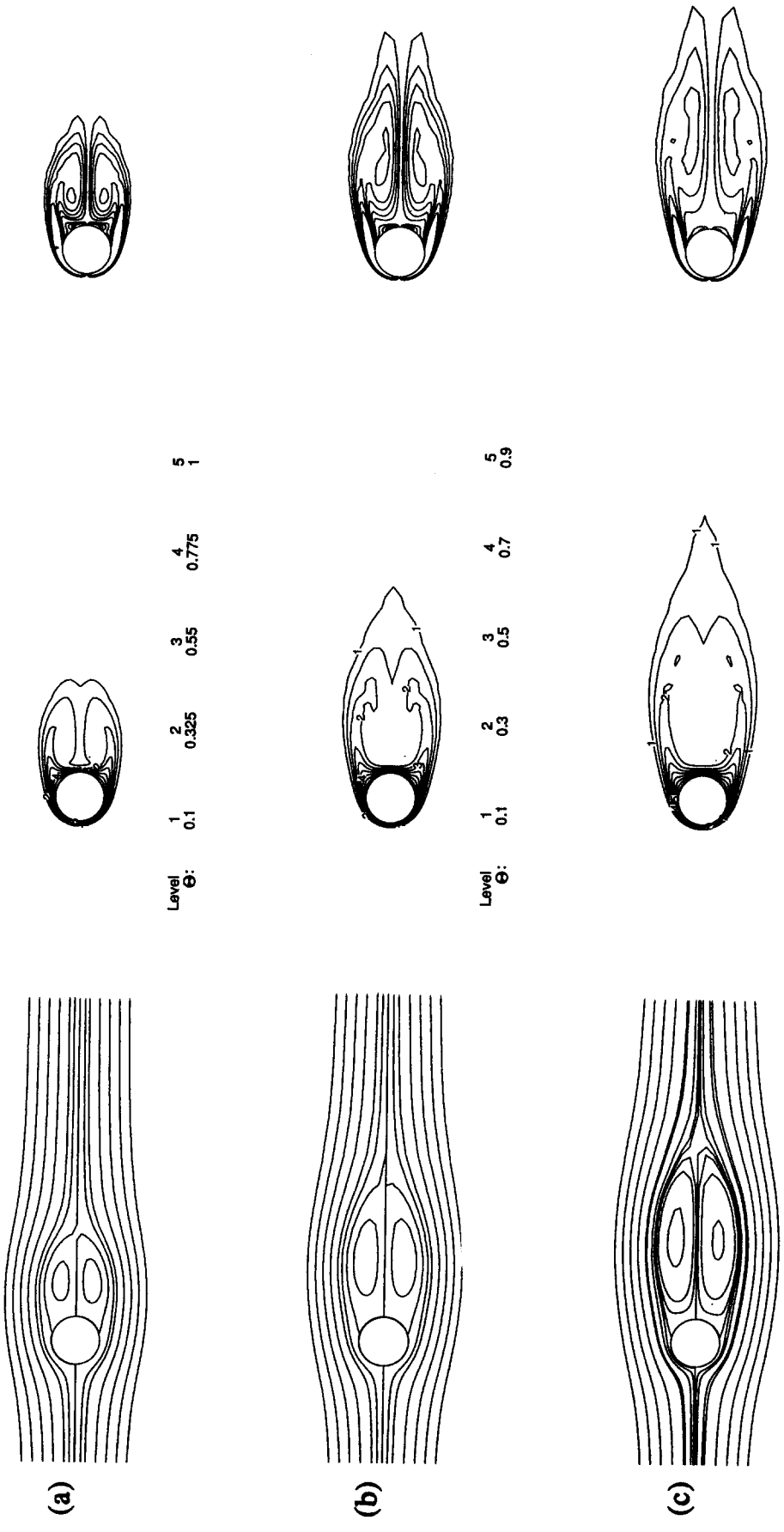

Fig. 2. Streamlines (left), temperature contours (middle) and vorticity contours (right) for case A: (a) $t = 10$, (b) $t = 20$ and (c) $t = 30$.

Table 3. Summary of simulation parameters with $Pr = 0.73$

Case	Re	Gr	δ	γ	ϕ	Ω_f
A	200	0	0	0	0	0
B	100	—	0	0	0.2	1.0
C	100	10^4	0	—	0.2	1.0
D	—	10^4	0	0.2	0.2	1.0
E	100	10^4	—	0.2	0.2	1.0

counter-clockwise direction. In general, they are all symmetric about the horizontal axis with the pressure being relatively low in the wake. It is worthwhile to note that only in the wake is the temporal development significant.

Shown in Figs. 4(a)–(c) are the three sets of streamlines and the isotherms corresponding to case B in Table 3 at $t = 40$. Here, the free-stream velocity and the gravity vector are perpendicular to each other, $\delta = 0$, so that the combined flow is normally referred to as a cross flow. In Fig. 4(a), the Grashof number is zero and vortex shedding, evidently triggered by the spinning motion of the cylinder, is seen to occur downstream. Such a phenomena results in a dispersion of warm fluid particles occuring alternately in a fashion similar to the von Karman vortex street. As soon as Gr becomes nonzero, an upward motion is induced causing a deflection of the streamlines in the wake as seen in Fig. (4b). Further increase in buoyancy force makes the rising convective currents strong enough to destroy the low pressure wake region; thereby preventing the formation of eddies behind the cylinder. Because of the absence of eddies, the shedding event cannot take place under the influence of a strong buoyancy force in cross flows.

Figures 5(a)–(c) illustrate the effects of rotation on the structure of the flow and temperature fields for case C at $t = 40$. Again, the deflection of the streamlines and isotherms is apparent and is attributed to the buoyancy force which in this case is comparable to the free stream velocity, i.e. $Gr/Re^2 = 1$ [see Fig. 5(b)]. When the cylinder is set in rotational motion, the streamlines and isotherms, especially in the wake, are somewhat modified from those of a stationary cylinder. Even though the magnitude of the angular velocity is one-half of the free stream velocity, it is the direction of rotation that is held accountable for two major dissimilarities. First, when rotation is in the clockwise direction the shearing motion tends to oppose the buoyancy force; hence the deflection

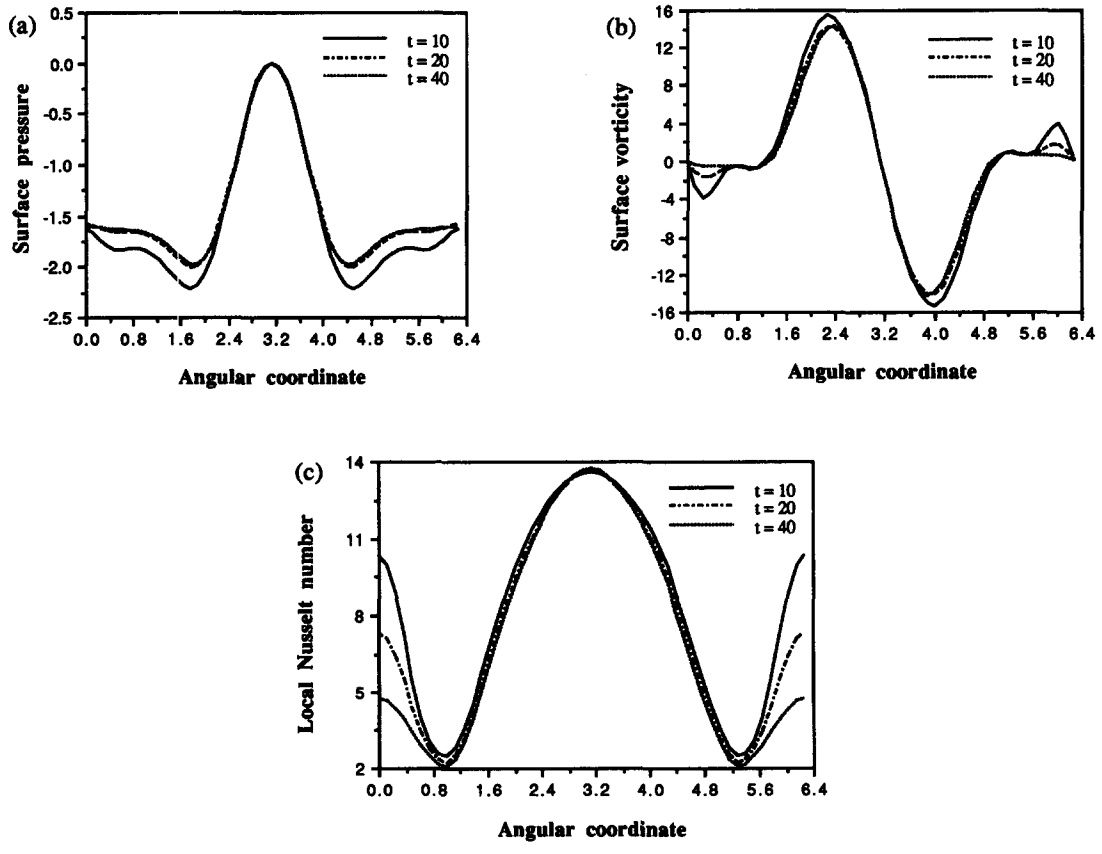

Fig. 3. Temporal development of surface quantities for case A: (a) pressure, (b) vorticity and (c) Nusselt number.

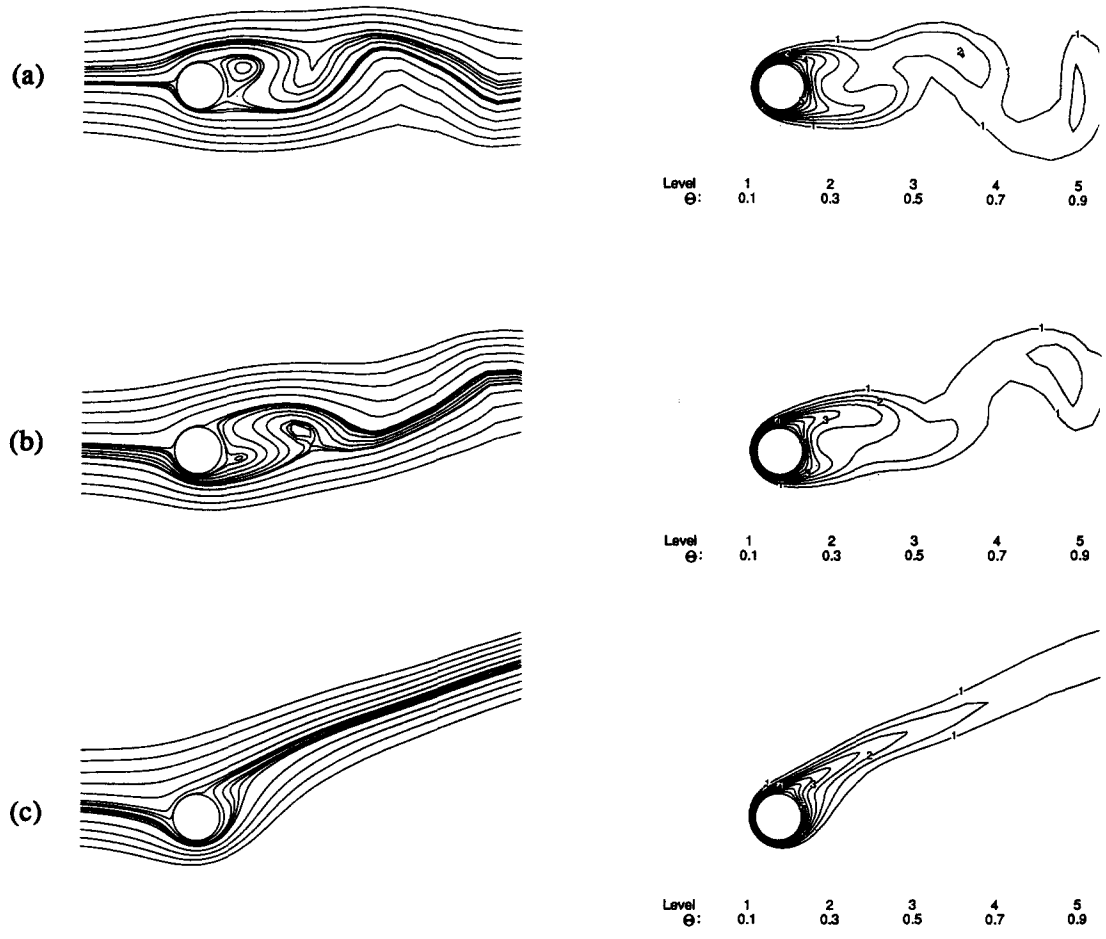

Fig. 4. Effects of Gr on streamlines and temperature contours for case B: (a) $Gr = 0$, (b) $Gr = 5 \times 10^3$ and (c) $Gr = 2 \times 10^4$.

becomes less. Conversely, when the cylinder spins in the counter-clockwise direction it adds momentum to the buoyancy-induced motion which, in turn, leads to higher deflection. Second, the weakening of the buoyancy-induced flow caused by cylinder rotation creates, behind the cylinder, secondary vortices which don't appear to be detached or shed.

In Figs. 6(a)–(c), case D, the Grashof number is fixed at 10^4 while the Reynolds number varies from 50 to 150. The trends observed in these figures are consistent with those in Figs. 4(a)–(c) where the Grashof number was kept constant. That is, a large Grashof number to Reynolds number squared ratio results in a high deflection of the streamlines and isotherms. As this ratio decreases by increasing the Reynolds number, the deflections become less and the streamlines in the wake deform into an S-shape and eventually eddies are developed and are detached from the surface as seen in Fig. 6(c).

Figures 7(a)–(c) show the effects due to flow orientation. In contrast to opposing ($\delta = \pi/2$) and cross ($\delta = 0$) flows, no deflection of the streamlines and the isotherms is detected in Fig. 7(b) for aiding ($\delta = 3\pi/2$) flow. This is because the line of action of buoyancy force is oriented parallel to the main flow. Owing to the buoyancy force having its direction the same as that of the free stream velocity, the combined motion has a higher acceleration, thus higher velocity, than either of the two alone. Consequently, the temperature plume becomes thinner and is lengthened in the streamwise direction as displayed in Fig. 7(b). This is anticipated since the gain in momentum allows fluid particles to be convected downstream further before their thermal energy is completely dissipated to the surrounding fluid. In Fig. 7(c) the gravity is now acting in the reverse direction ($\delta = \pi/2$); thus producing a resisting buoyant motion. As a result, the flow and temperature fields are quite distinct from that seen in Figs. 7(a) and (b). Here, the momentum loss resulting from flow cancellation leads to an expansion of the thermal plume in the direction normal to the free-stream velocity.

In order to quantify the effects of Gr, Re, γ and δ on the heat transfer, the local Nusselt number and the overall Nusselt number are plotted in Figs. 8(a)–(d) and Figs. 9(a)–(d), respectively, for the cases con-

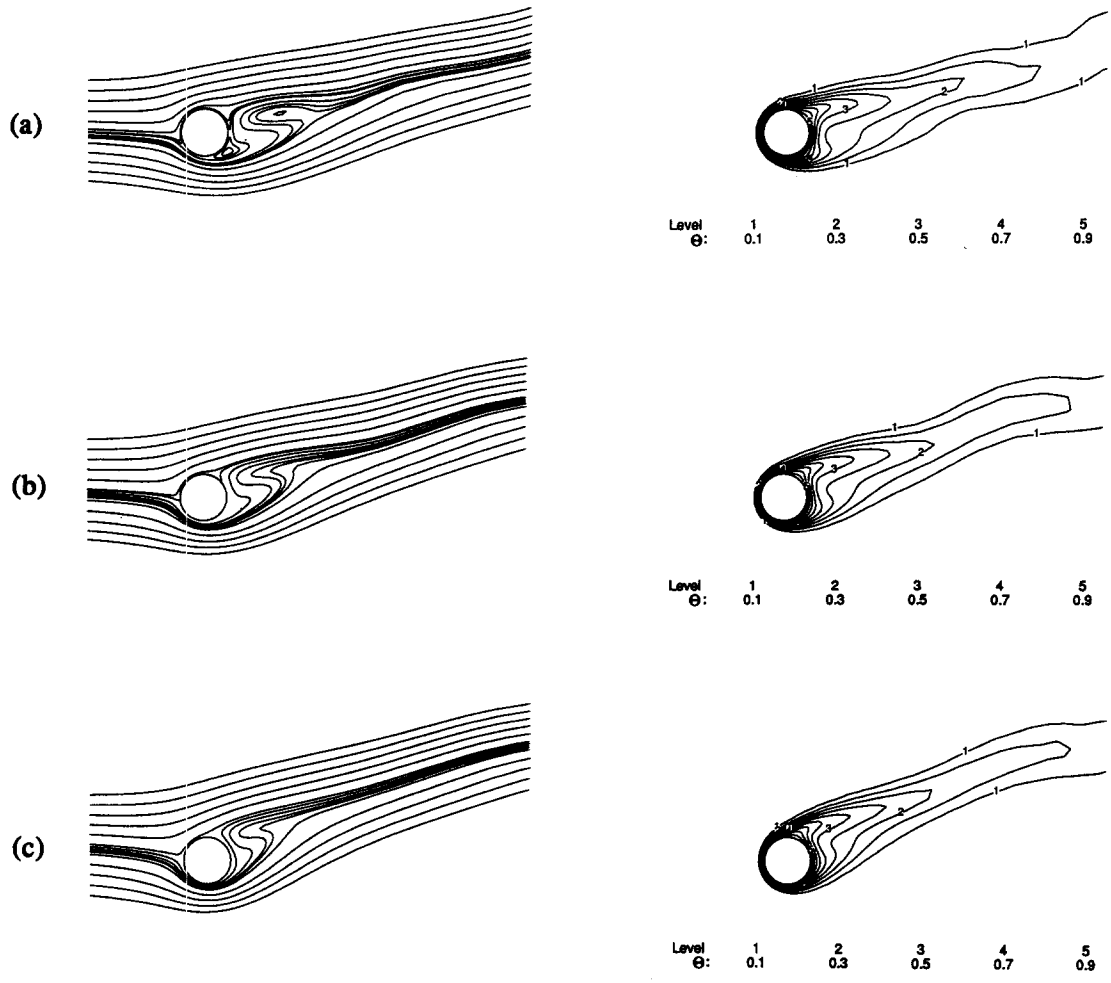

Fig. 5. Effects of γ on streamlines and temperature contours for case C: (a) $\gamma = -0.5$, (b) $\gamma = 0$ and (c) $\gamma = 0.5$.

sidered in the above parametric study. For cross flows and for a given Reynolds number, the total heat transfer rate increases as the Grashof number increases [see Fig. 8(a)]. This enhancement mainly comes from the lower half of the cylinder where a pronounced increase of heat flux is experienced. Though the heat flux along the other half of the cylinder surface is not very sensitive to the Grashof number, it is interesting to note a reduction of the heat flux in the region next to the wake. As for the effects due to the cylinder rotation, a positive rotation simply shifts the local Nusselt number curve to the right whereas a negative rotation shifts it to the left. Also observed in Fig. 8(b) is a depression or elevation of the Nusselt number curves depending on the direction of rotation. If the direction is positive, the buoyancy is enhanced and the curve is elevated. Nonetheless, the depression or elevation is small and the area under these curves, i.e. the overall Nusselt number, therefore differs relatively little at least for the range of γ from -0.5 to 0.5 as revealed in Fig. 9(b). Figures 8(c) and 9(c) show the heat transfer performance under varying Reynolds numbers. In general, the local Nusselt number shows higher values everywhere along the cylinder surface for higher Reynolds numbers except as usual in the wake where no definite trend can be discerned. Correspondingly, the overall Nusselt number is an increasing function of the Reynolds number. Among the parameters considered in this study, none appears to produce a more dramatic change in the heat transfer rate than the gravitational orientation [see Fig. 8(d)]. Once again, the increase in the local Nusselt number for the case of aiding flow is another evidence of the buoyancy enhancement. When the gravity and the free stream velocity are colinear and pointing in the same direction (as for the case of opposing flow), the shape of the local Nusselt number profile changes drastically. Another interesting feature about the effects due to gravitational orientation is the transient behavior of the Nusselt number history in opposing flows where it exhibits a dip and its value at long time seems much closer to that for cross flow than one would expect.

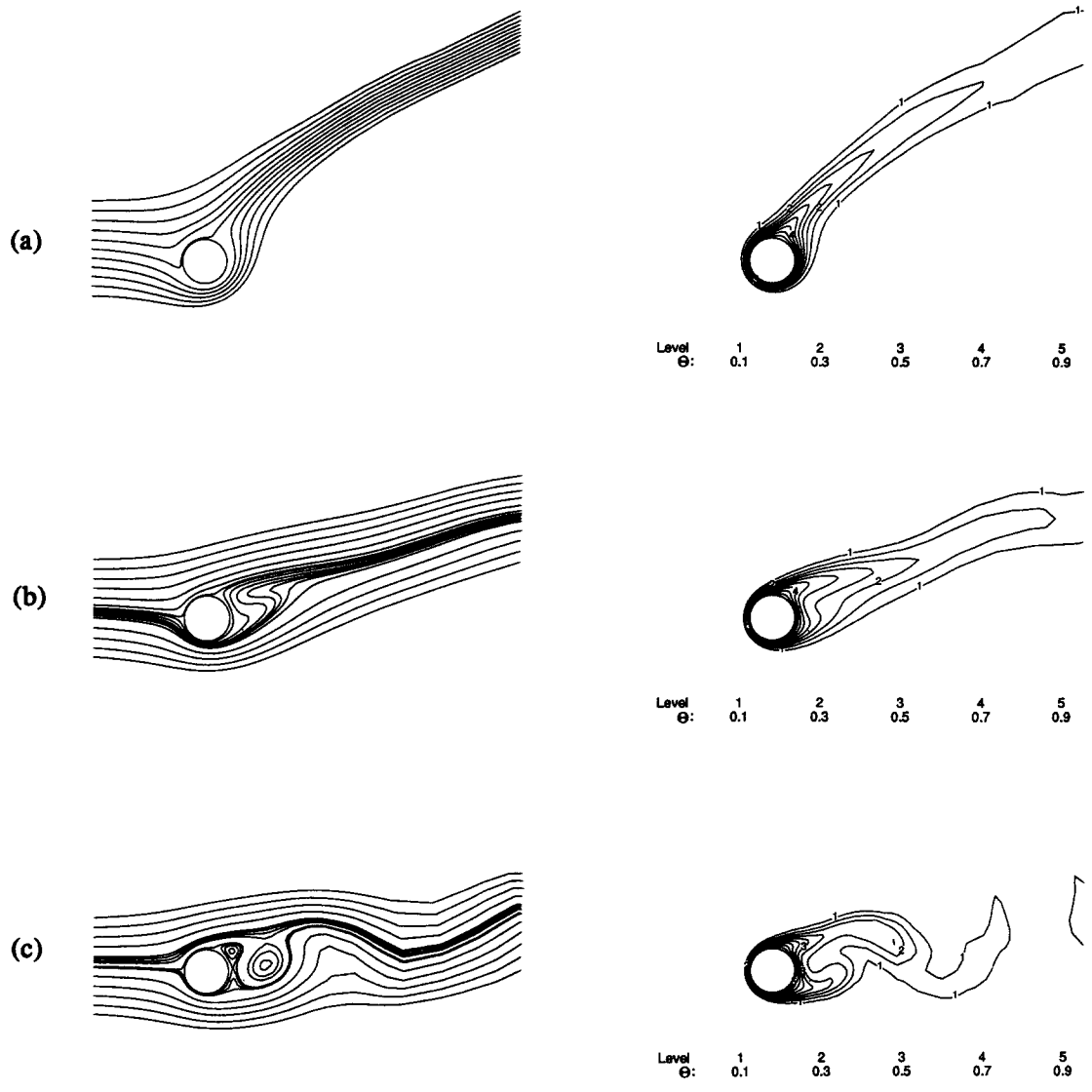

Fig. 6. Effects of Re on streamlines and temperature contours for case D: (a) $Re = 50$, (b) $Re = 100$ and (c) $Re = 150$.

All Nusselt number history curves presented in Figs. 9(a)–(d) have one feature in common: an oscillatory period preceded by a non-oscillating period. The former is a direct consequence of the oscillations in the main flow whereas the latter is a result of conduction mechanism that is usually dominant during the early stage of the transport process.

5. CONCLUDING REMARKS

Heat transfer in the presence of forced convection, free convection, body rotation with flow pulsation is investigated numerically using a Fourier-spectral element method. A parametric study is performed to quantify the effects due to the buoyancy force under vortex shedding conditions. Conclusions can be summarized as follows:

(1) For pure forced convection up to $Re = 200$, asymmetry of the wake exists, but vortex shedding was not observed for dimensionless time up to 40.

(2) Augmentation of heat transfer can be accomplished by several means including an increase in the Grashof number and/or Reynolds numbers.

(3) Depending on the direction of rotation, a small increase or decrease in the Nusselt number can be obtained if the direction is to aid or oppose the buoyancy force.

(4) With regards to the direction of the gravity, Nusselt number is highest in aiding flow and lowest in opposing flow.

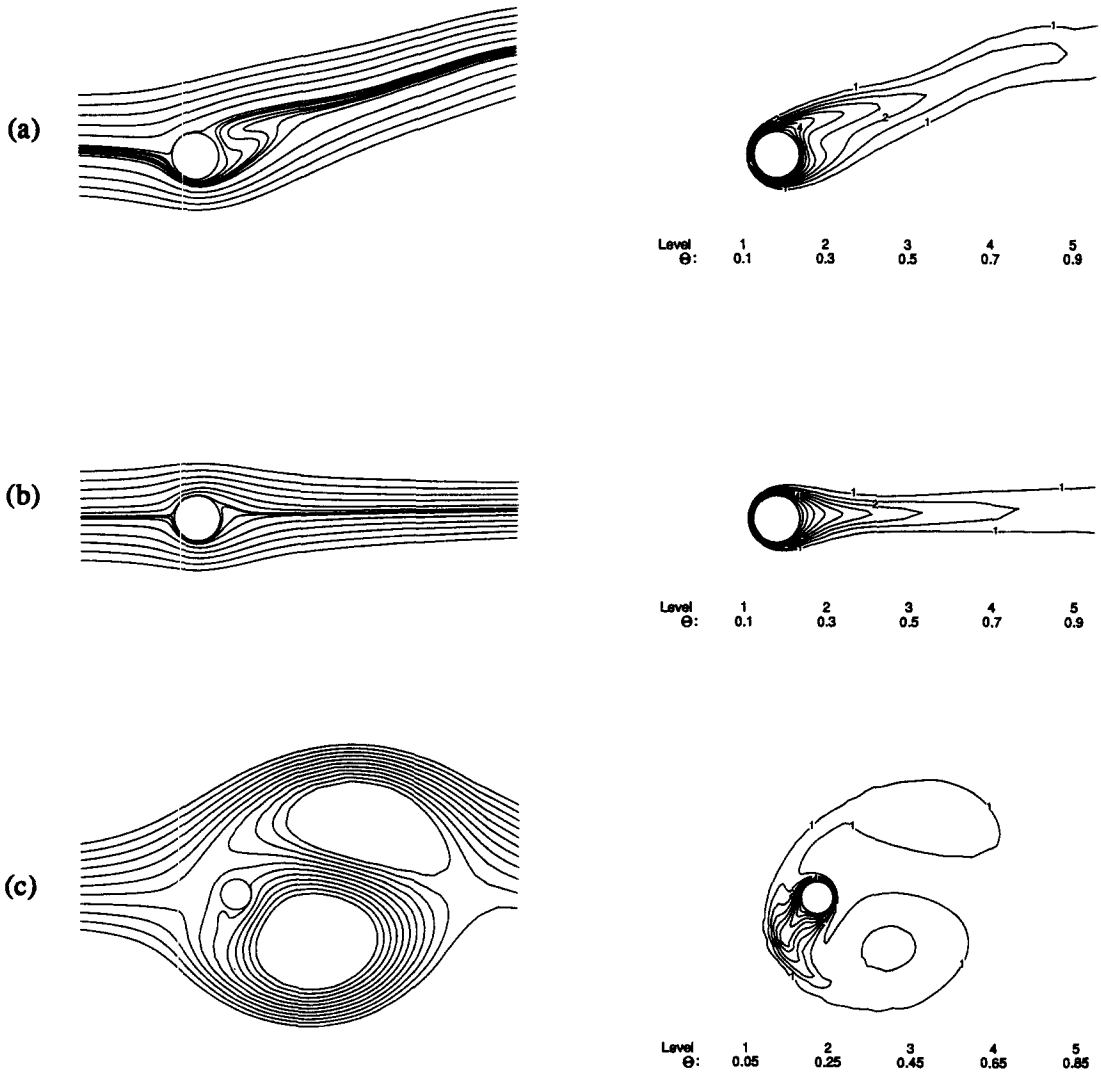

Fig. 7. Effects of δ on streamlines and temperature contours for case E: (a) $\delta = 0$, (b) $\delta = 3\pi/2$ and (c) $\delta = \pi/2$.

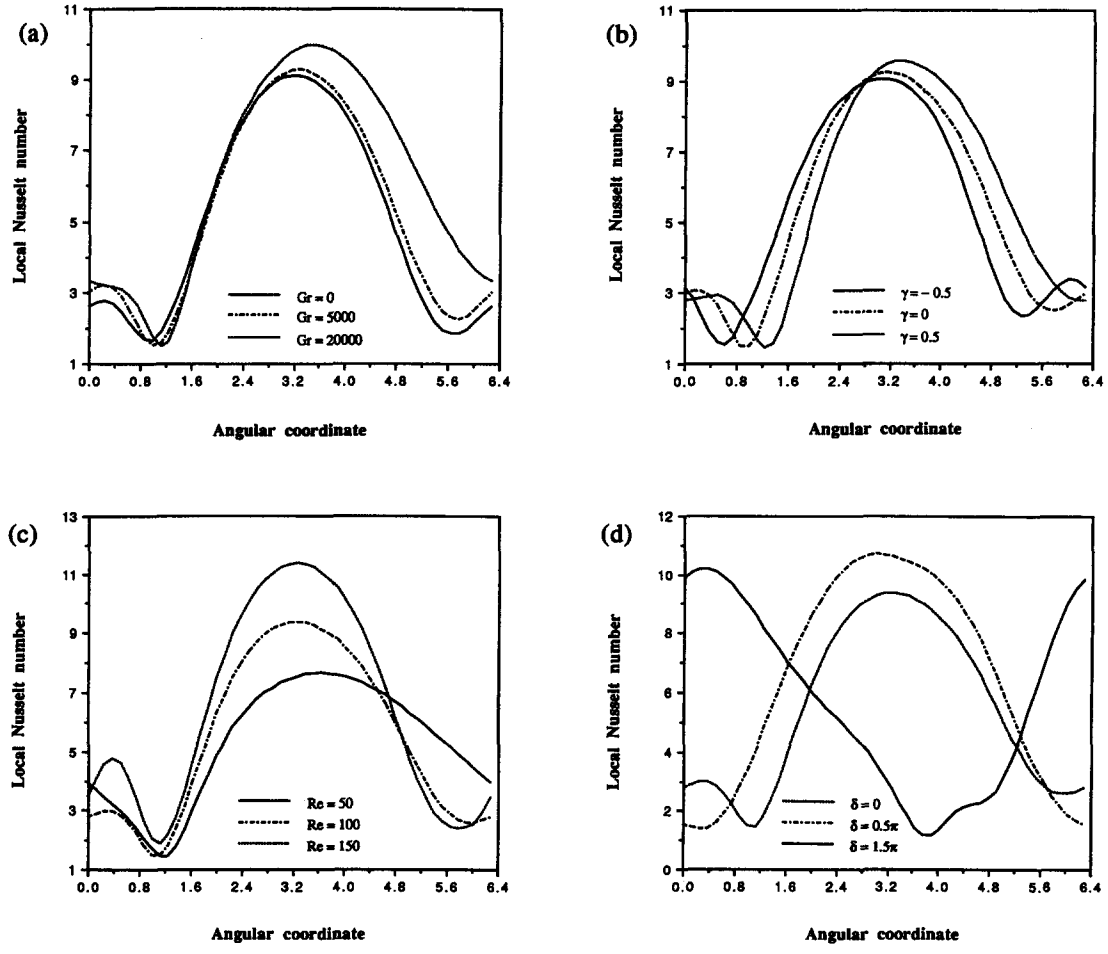

Fig. 8. Local Nusselt numbers: (a) case B, (b) case C, (c) case D and (d) case E.

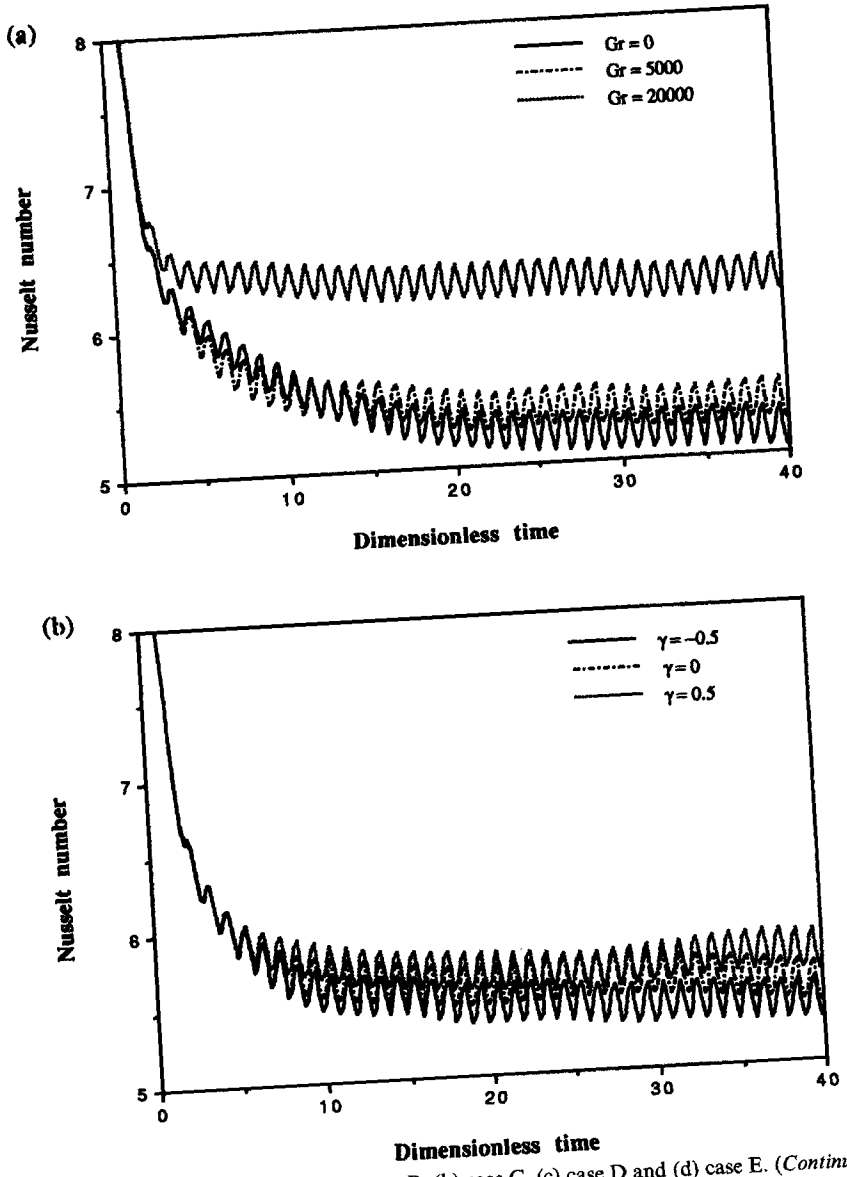

Fig. 9. History of mean Nusselt numbers: (a) case B, (b) case C, (c) case D and (d) case E. (*Continued overleaf.*)

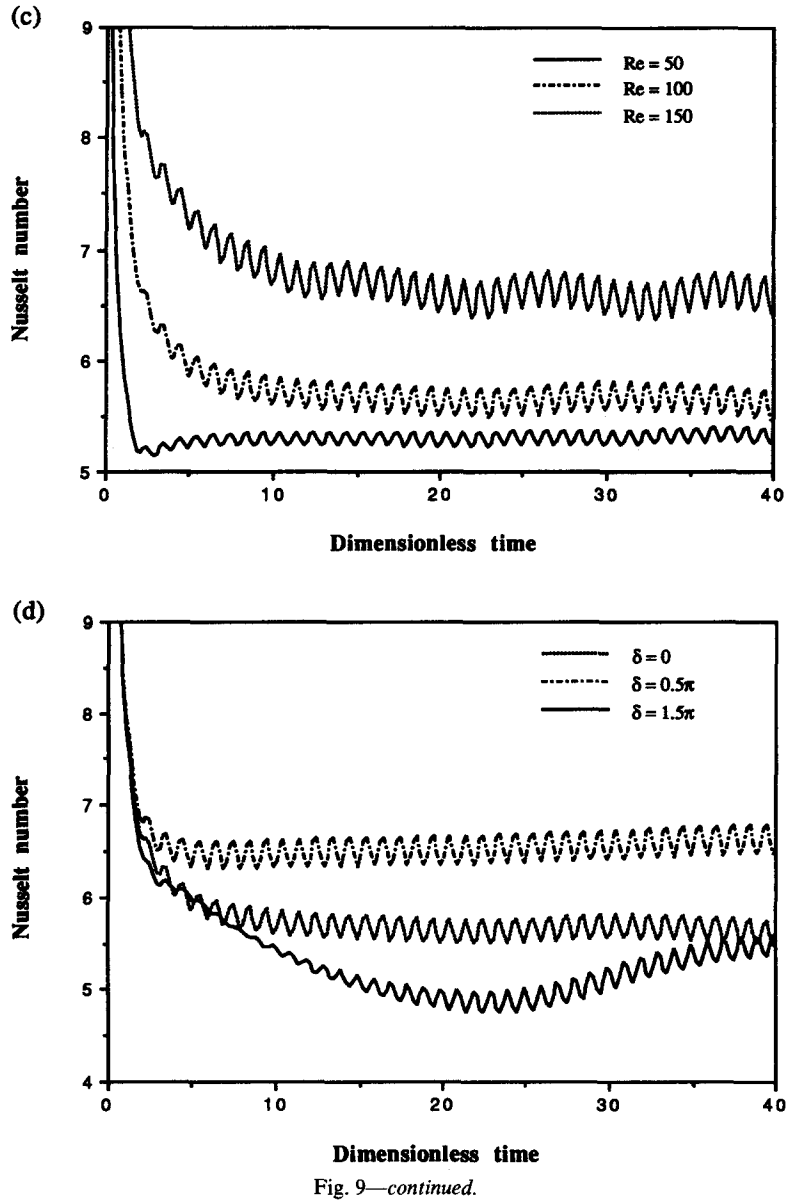

Fig. 9—*continued.*

Acknowledgement—This work is performed under the auspices of the U.S. Department of Energy, contract DE-AC07-94ID13223 through the support of the INEL Long-Term Research Initiative in Computational Mechanics.

REFERENCES

1. V. T. Morgan, The overall convective heat transfer from smooth circular cylinders, *Adv. Heat Transfer* **11**, 199–264 (1975).
2. S. C. R. Dennis, J. D. Hudson and N. Smith, Steady laminar forced convection from a circular cylinder at low Reynolds numbers, *Physics Fluids* **11**, 933–940 (1967).
3. P. C. Jain and B. S. Goel, A numerical study of unsteady laminar forced convection from a circular cylinder, *J. Heat Transfer* **98**, 303–307 (1976).
4. G. E. Karniadakis, B. B. Mikic and A. T. Patera, Unsteady heat transfer from a cylinder in cross flow; a direct numerical simulation, *Heat Transfer* **2**, 429–434 (1986).
5. Z. H. Qureshi and R. A. Ahmad, Natural convection from a horizontal cylinder at moderate Rayleigh numbers, *Numer. Heat Transfer* **11**, 199–212 (1987).
6. S. Kimura and I. Pop, Conjugate natural convection from a horizontal circular cylinder, *Numer. Heat Transfer* **25A**, 347–361 (1994).
7. P. C. Jain and B. L. Lohar, Unsteady mixed convection heat transfer from a horizontal circular cylinder, *J. Heat Transfer* **101**, 126–131 (1979).
8. H. M. Badr, A theoretical study of laminar mixed convection from a horizontal cylinder in a cross stream, *Int. J. Heat Mass Transfer* **26**, 639–653 (1983).
9. R. A. Ahmad and Z. H. Qureshi, Laminar mixed convection from a uniform heat flux horizontal cylinder in

a crossflow, *J. Thermophys. Heat Transfer* **6,** 277–287 (1992).
10. V. A. Patel, Karman vortex street behind a circular cylinder by the series truncation method, *J. Comput Phys.* **28,** 14–42 (1978).
11. H. M. Badr and S. C. R. Dennis, Time-dependent viscous flow past an impulsively started rotating and translating circular cylinder, *J. Fluid Mech.* **158,** 447–488 (1985).
12. H. M. Badr, M. Coutanceau, S. C. R. Dennis and C. Menard, Unsteady flow past a rotating circular cylinder at Reynolds numbers 10^3 and 10^4, *J. Fluid Mech.* **220,** 459–484 (1990).
13. D. B. Ingham and T. Tang, A numerical investigation into the steady flow past a rotating circular cylinder at low and intermediate Reynolds numbers, *J. Comput. Phys.* **87,** 91–107 (1990).
14. T. Tang and D. B. Ingham, On steady flow past a rotating circular cylinder at Reynolds numbers 60 and 100, *Comput. Fluids* **19,** 217–230 (1991).
15. H. M. Badr and S. C. R. Dennis, Laminar forced convection from a rotating cylinder, *Int. J. Heat Mass Transfer* **28,** 253–264 (1985).
16. H. D. Nguyen, S. Paik and R. W. Douglass, A Legendre-spectral element method for flow and heat transfer about an accelerating droplet, *J. Sci. Comput.* (submitted).
17. W. H. McAdams, *Heat Transmission.* McGraw-Hill, New York (1954).
18. B. Gebhart, Y. Yaluria, R. L. Mahajan and B. Samakia, *Buoyancy-induced Flows and Transport*, Chap. 10, pp. 490–491. Hemisphere, New York (1988).

APPENDIX

We here briefly summarize the expressions for the buoyancy and the convective terms as abbreviated in equations (10)–(13). These are

$$BG_0 = \frac{Gr}{4Re}\left\{\cos\delta\left[r\frac{dH_1}{dr}+H_1\right]-\sin\delta\left[r\frac{dh_1}{dr}+h_1\right]\right\} \tag{A1}$$

$$BG_n = \frac{Gr}{8Re}\left\{\cos\delta\left[r\left(\delta_{n1}\frac{dH_0}{dr}+\frac{dH_{n+1}}{dr}+\frac{dH_{n-1}}{dr}\right)+(n+1)H_{n+1}-(n-1)H_{n-1}\right]-\sin\delta\left[r\left(\frac{dh_{n+1}}{dr}-\frac{dh_{n-1}}{dr}\right)+(n+1)h_{n+1}+(n-1)h_{n-1}\right]\right\} \tag{A2}$$

$$Bg_n = \frac{Gr}{8Re}\left\{\cos\delta\left[r\left(\frac{dh_{n+1}}{dr}+\frac{dh_{n-1}}{dr}\right)+(n+1)h_{n+1}-(n-1)h_{n-1}\right]-\sin\delta\left[r\left(\delta_{n1}\frac{dH_0}{dr}-\frac{dH_{n+1}}{dr}+\frac{dH_{n-1}}{dr}\right)-(n+1)H_{n+1}-(n-1)H_{n-1}\right]\right\} \tag{A3}$$

$$SG_0 = 2\sum_{m=1}^{N} m\left(F_m\frac{dg_m}{dr}-f_m\frac{dG_m}{dr}+g_m\frac{dF_m}{dr}-G_m\frac{df_m}{dr}\right) \tag{A4}$$

$$SG_n = -nf_n\frac{dG_0}{dr}+ng_n\frac{dF_0}{dr}+\sum_{m=1}^{N}\left\{\frac{dg_m}{dr}[KF_K+(m-n)F_J]-\frac{dG_m}{dr}[Kf_K+Jf_J]+mg_m\left[\frac{dF_K}{dr}+\frac{dF_J}{dr}\right]-mG_m\left[\frac{df_K}{dr}+\sin(m-n)\frac{df_J}{dr}\right]\right\} \tag{A5}$$

$$Sg_n = nF_n\frac{dG_0}{dr}-nG_n\frac{dF_0}{dr}+\sum_{m=1}^{N}\left\{\frac{dg_m}{dr}(Kf_K-Jf_J)+\frac{dG_m}{dr}[KF_K-(m-n)F_J]+mg_m\left[\frac{df_K}{dr}-\sin(m-n)\frac{df_J}{dr}\right]+mG_m\left[\frac{dF_K}{dr}-\frac{dF_J}{dr}\right]\right\} \tag{A6}$$

$$SH_0 = 2\sum_{m=1}^{N} m\left(F_m\frac{dh_m}{dr}-f_m\frac{dH_m}{dr}+h_m\frac{dF_m}{dr}-H_m\frac{df_m}{dr}\right) \tag{A7}$$

$$SH_n = -nf_n\frac{dH_0}{dr}+nh_n\frac{dF_0}{dr}+\sum_{m=1}^{N}\left\{\frac{dh_m}{dr}[KF_K+(m-n)F_J]-\frac{dH_m}{dr}[Kf_K+Jf_J]+mh_m\left[\frac{dF_K}{dr}+\frac{dF_J}{dr}\right]-mH_m\left[\frac{df_K}{dr}+\sin(m-n)\frac{df_J}{dr}\right]\right\} \tag{A8}$$

$$Sh_n = nF_n\frac{dH_0}{dr}-nH_n\frac{dF_0}{dr}+\sum_{m=1}^{N}\left\{\frac{dH_m}{dr}[KF_K-(m-n)F_J]+\frac{dh_m}{dr}[Kf_K-Jf_J]+mh_m\left[\frac{df_K}{dr}-\sin(m-n)\frac{df_J}{dr}\right]+mH_m\left[\frac{dF_K}{dr}-\frac{dF_J}{dr}\right]\right\} \tag{A9}$$

where $K = m+n$, $J = |m-n|$ and $\sin(m-n)$ is the sine of $(m-n)$.